Bioconjugate Chemistry

Article

pubs.acs.org/bc

# Quantitative Assessment of Binding Affinities for Nanoparticles Targeted to Vulnerable Plaque

Tang Tang,[†] Chuqiao Tu,[‡] Sarah Y. Chow,[§] Kevin H. Leung,[‡] Siyi Du,[†] and Angelique Y. Louie*[,‡]

Departments of [†]Chemistry, [‡]Biomedical Engineering, and [§]Chemical Engineering, University of California, Davis, California 95616, United States

Supporting Information

**ABSTRACT:** Recent successes in targeted immune and cell-based therapies have driven new directions for pharmaceutical research. With the rise of these new therapies there is an unfilled need for companion diagnostics to assess patients' potential for therapeutic response. Targeted nanomaterials have been widely investigated to fill this niche; however, in contrast to small molecule or peptide-based targeted agents, binding affinities are not reported for nanomaterials, and to date there has been no standard, quantitative measure for the interaction of targeted nanoparticle agents with their targets. Without a standard measure, accurate comparisons between systems and optimization of targeting behavior are challenging. Here, we demonstrate a method for quantitative assessment of the binding affinity for targeted nanoparticles to cell surface receptors in living systems and apply it to optimize the development of a novel targeted nanoprobe for imaging vulnerable atherosclerotic plaques. In this work, we developed sulfated dextran-coated iron oxide nanoparticles with specific targeting to macrophages, a cell type whose density strongly correlates with plaque vulnerability. Detailed quantitative, *in vitro* characterizations of $^{111}In^{3+}$ radiolabeled probes show high-affinity binding to the macrophage scavenger receptor A (SR-A). Cell uptake studies illustrate that higher surface sulfation levels result in much higher uptake efficiency by macrophages. We use a modified Scatchard analysis to quantitatively describe nanoparticle binding to targeted receptors. This characterization represents a potential new standard metric for targeted nanomaterials.

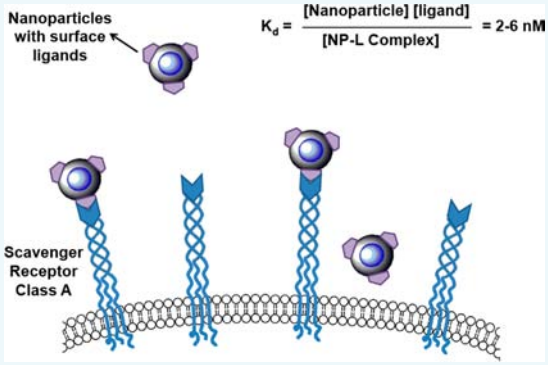


## INTRODUCTION

Nanomaterials have been widely investigated for use as diagnostic agents and carriers for therapeutics. The ability to tune to nanometer size ranges has been ascribed to beneficial properties for health applications, including avoidance of rapid kidney clearance, increased circulation time, and the delivery of high payloads of imaging agents or drugs.[1,2] This class of materials holds great potential for clinical application, but assessment for the efficacy of nanomaterials for biological applications has lacked quantitative rigor and largely depended upon qualitative comparison of changes in image intensity or therapeutic effect.[3] Unlike small molecule or macromolecule counterparts, nanomaterial binding affinities are typically not reported. Without this information, there is a lack of precision in attempts to improve target recognition. Quantitative assessments can help to inform design optimization of target binding and cellular recognition as well as provide a yardstick against which other nanomaterials can be compared.

In a handful of examples, surface plasmon resonance or quartz crystal microbalance with dissipation monitoring were utilized for characterization of particle binding affinities, but these methods assay the binding of nanoparticles to isolated proteins that are immobilized on sensor chips. This need for purified immobilized targets has a number of drawbacks.[4,5] The unnatural presentation of the target may not reflect the actual interactions between nanoparticles and their target of interest found *in vitro* or *in vivo*. Also, the purification and immobilization of analyte proteins to sensor chips present substantial technical challenges and research effort, particularly for transmembrane proteins. Thus, there remains a critical need to develop other methods for quantitative *in vitro* measurements of binding affinity of nanomaterials to their targets, especially for membrane-localized receptors. In this work, we develop nanoparticles targeted to cell surface receptors found on activated macrophages and adapt Scatchard analysis to characterize the binding affinities of the nanoparticles to these receptors.

We have previously reported on multimodal positron emission tomography and magnetic resonance imaging (PET/MRI) probes targeted to macrophages that accumulated in inflamed plaques in a rodent injury model.[6−8] These probes are sulfated dextran-coated iron oxide nanoparticles (SDIO); surface sulfation allows specific targeting to macrophages through the scavenger receptor class A (SR-A) that recognizes dextran sulfate.[6−8] The scavenger receptor class A is considered to be one of the primary receptors responsible for modified

**Received:** March 18, 2015
**Revised:** April 29, 2015
**Published:** May 13, 2015





DOI: 10.1021/acs.bioconjchem.5b00144
*Bioconjugate Chem.* 2015, 26, 1086−1094

**Scheme 1. Synthesis of SDIO−DO3A Nanoparticles**[a]

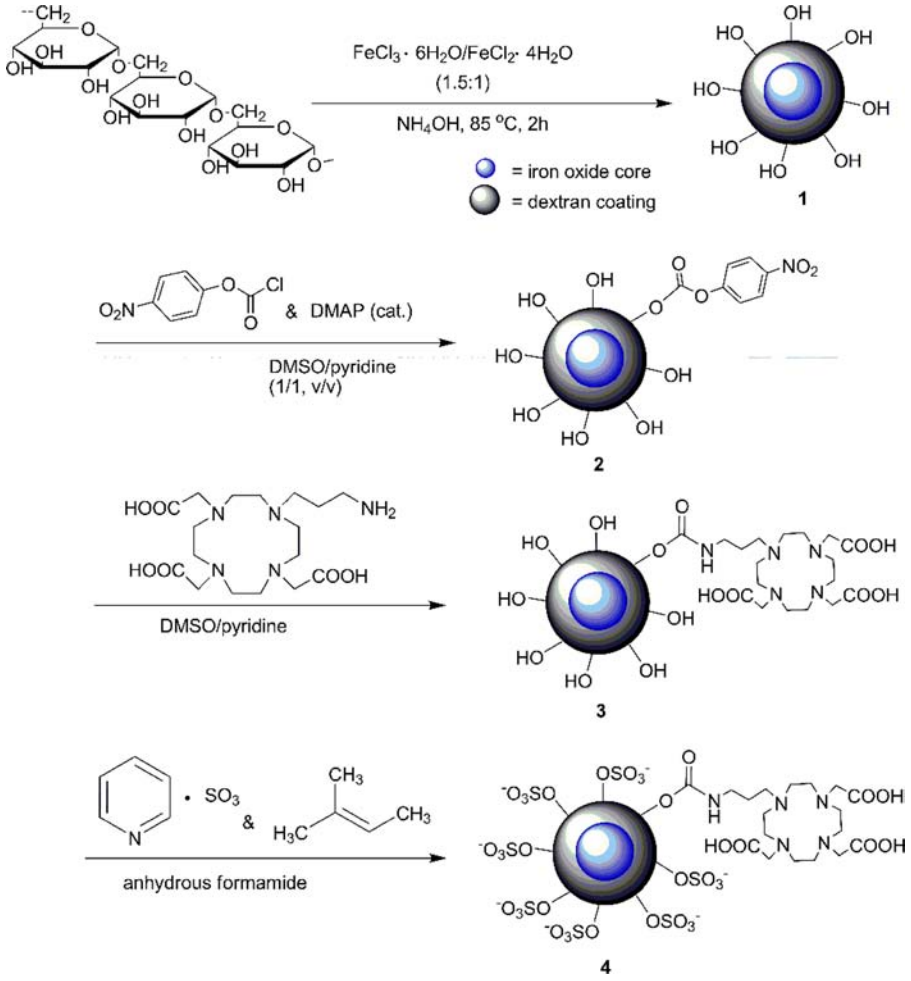


[a]DMAP, 4-(dimethylamino) pyridine. In this new method, conjugation of the chelator is achieved by directly coupling to the hydroxyl groups without a requirement of cross-linking and amination. Sulfation is realized after conjugation of the chelator to maximize the sulfation degree.

lipoprotein uptake by macrophages, a key factor in the development of atherosclerosis.[9] SR-A is unique to activated macrophages in inflamed vessel lumens[9,10] and interacts with a broad variety of polyanionic ligands such as maleylated bovine serum albumin.[11,12] It can internalize bound ligands rapidly and repeatedly recycle through the endosomal compartment on the order of 10 min.[13−15] Its unique, high expression and efficient uptake suggest a capacity for ligand accumulation that makes SR-A an ideal target for probe design.

Given the scavenger receptor's preference for polyanionic ligands such as dextran sulfate and our previous observation that increasing negative charge improves the binding of maleylated bovine serum albumin (mal-BSA) to SR-A,[16] we hypothesized that increased surface sulfation on the dextran coating of the probes would improve binding and cellular uptake.[12] Herein, we developed a series of SDIO nanoparticles with increased sulfation levels and performed quantitative investigation of the effect of different levels of sulfation on target binding and macrophage cellular uptake efficiency. We describe radiolabeling studies to assess the binding affinities of these SDIO nanoparticles using Scatchard analysis. Studying these binding affinities could help elucidate how to optimize attachment of the targeting ligands to the nanoparticles for maximum recognition of target and permit assessment of multivalency effects that could occur with multiple ligands presented on the surface of the particle.

## RESULTS

**Synthesis and Characterization of SDIO−DO3As.** The synthetic route for SDIO−DO3A nanoparticles is shown in Scheme 1. Dextran-coated iron oxide nanoparticles (DIO) were synthesized by a coprecipitation method as previously reported.[7] To achieve a multimodal function, we conjugated a chelator with high stability for copper ions and used a simple chelation process for our iron oxide nanoparticles. Although DOTA (1,4,7,10-tetraazacyclododecane-1,4,7,10-tetraacetic acid) is one of the most commonly used *in vivo* ligands for chelation of metals such as $^{64}Cu^{2+}$, $Gd^{3+}$, and $^{111}In^{3+}$ ($Cu^{2+}$-DOTA, log $K$ = 22; $In^{3+}$-DOTA, log $K$ = 23.9),[17−19] the commercially available *p*-SCN-Bn-DOTA was difficult to conjugate to DIOs in our previous experience.[20,21] This is likely due to the steric hindrance caused by the short and rigid arm of SCN-Bn. Therefore, we previously developed a new bifunctional DO3A (1,4,7,10-tetraazacyclododecane-1,4,7-triacetic acid) derivative ($Cu^{2+}$-DO3A, log $K$ = 26)[22,23] that has a more flexible aliphatic amine for attachment to the DIO and applied it in this work.[21,24] Conjugation of the chelator is a two-step reaction directly coupling to the hydroxyl groups in the



DOI: 10.1021/acs.bioconjchem.5b00144
*Bioconjugate Chem.* 2015, 26, 1086−1094

**Table 1. Physical Properties of SDIO−DO3A in Comparison to Those of DIO−DO3A**

| nanoparticles (with S/OH ratio) | core size (nm) | hydrodynamic diameter (nm) | % S | % Fe | zeta potential $\zeta$ (mV) DI | zeta potential $\zeta$ (mV) PBS | relaxivity ($mM^{-1}$ $s^{-1}$)[b] $r_1$ | relaxivity ($mM^{-1}$ $s^{-1}$)[b] $r_2$ |
|---|---|---|---|---|---|---|---|---|
| DIO−DO3A | 5.9 ± 1[a] | 22.9 ± 6.7 | 0 | 19.7 | 11.7 | −5.6 | 17.9 | 103.3 |
| SDIO−DO3A-0.2 | 5.8 ± 1 | 33.4 ± 7.5 | 0.42 | 19.4 | −19.5 | −8.8 | 16.3 | 87.6 |
| SDIO−DO3A-1 | 5.7 ± 1 | 44.2 ± 10.4 | 3.41 | 20.1 | −34.3 | −11.8 | 15.8 | 81.8 |
| SDIO−DO3A-5 | 5.9 ± 1 | 62.7 ± 18.8 | 9.89 | 10.3 | −45.1 | −21.7 | 14.8 | 75.6 |
| SDIO−DO3A-10 | 5.9 ± 1 | 64.4 ± 17.5 | 11.32 | 10.6 | −44.6 | −25.2 | 14.2 | 72.8 |

[a]Data presented with standard deviation. [b]Measurement done at 1.4 T, 37 °C.

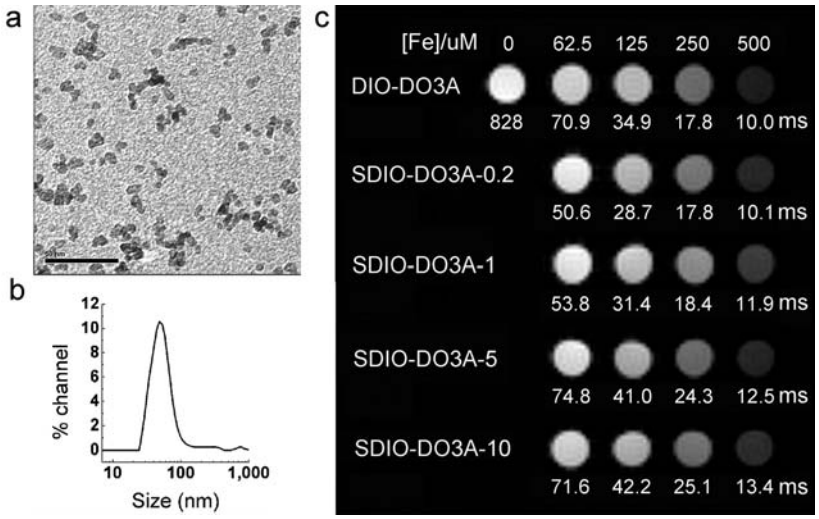


**Figure 1.** Physical properties of SDIO−DO3A nanoparticles. (a) TEM image shows iron oxide cores of SDIO−DO3A-10 nanoparticles, with average size of 5.9 nm. Scale bar: 50 nm. (b) Hydrodynamic size distribution of SDIO−DO3A-10 was obtained by dynamic light scattering, with average diameter (volume weighted) of 64.4 ± 17.5 nm (SD) and a single peak at 50.6 nm. (c) $T_2$-weighted MR image of DIO−DO3A and SDIO−DO3A aqueous solutions at 7 T (MSME, TR = 5000 ms, TE = 35 ms). From top to bottom, the rows represent DIO−DO3A, SDIO−DO3A-0.2, SDIO−DO3A-1, SDIO−DO3A-5, and SDIO−DO3A-10 solutions, respectively, at iron concentrations of 67.5, 125, 250, and 500 $\mu$M from left to right, including a blank (PBS solution). The $T_2$ values are shown underneath each sample. As expected, a concentration-dependent decrease in signal is observed for all nanoparticles, with similar performance.

dextran coating; this avoids the steps required for cross-linking and amination of the hydroxyl groups found in other bioconjugation approaches.[20,25] We sulfated the dextran coating after conjugation of the chelator to maximize the sulfate level on the surface. It has been reported in the literature that a ratio up to 10:1 can accomplish high sulfation of polysaccharides.[26] We used four different ratios of sulfur trioxide pyridine complex to hydroxyl groups on dextran (1:5, 1:1, 5:1, 10:1) and successfully synthesized a series of SDIO nanoparticles with different degrees of sulfation. The nanoparticles are denoted SDIO−DO3A-0.2, SDIO−DO3A-1, SDIO−DO3A-5, and SDIO−DO3A-10, corresponding to the ratio of sulfur trioxide to hydroxyls on dextran.

SDIO−DO3A nanoparticles were verified by elemental analysis and infrared spectroscopy. The emergence of sulfur content and new absorption peaks such as an asymmetrical S═O stretch at 1221 $cm^{-1}$ in the IR spectrum (Supporting Information, Figure S1) confirmed successful sulfation. The elemental analysis results showed that with a 10:1 ratio of $SO_3$ pyridine complex to hydroxyls on dextran (S/OH), the surface achieved the highest degree of sulfation, with sulfur content (by total mass) of 11.32%, compared to 9.89% (5:1), 3.41% (1:1), and 0.42% (1:5). These results are summarized in Table 1 and verify that an increased S/OH ratio greatly improved the surface sulfation of the nanoparticles.

Core sizes of the five different nanoparticles were measured by TEM and found to be ∼5.8 ± 1 nm in diameter ($n$ = 500 particles) (Figure 1a). Hydrodynamic diameters for the SDIO−DO3A nanoparticles were observed by dynamic light scattering as in Figure 1b. Generally, SDIO−DO3A had larger hydrodynamic sizes than DIO−DO3A, and hydrodynamic size increased with degree of sulfation, whereas the core sizes stayed the same. This is likely due to the repulsion of negatively charged sulfate groups on the surface causing the polysaccharide coat to expand slightly. A size distribution for SDIO−DO3A-10 is shown in Figure 1b as an example, with a diameter (volume weighted) of 64.4 ± 17.5 nm and a peak at 50.6 nm. The consistent core sizes suggest that once the iron oxide cores are formed, surface modification has little effect on the core sizes. This is also in agreement with our previous results with DIO that were modified with maleic anhydride.[27]

Zeta potentials of SDIO−DO3As were measured in deionized water and phosphate buffered saline, as shown in Table 1. There is a trend that higher sulfation levels resulted in more negative zeta values, until about −45 mV for both SDIO−DO3A-5 and SDIO−DO3A-10, suggesting a saturation of sulfate groups on the surface. SDIO−DO3-10 has a high negative zeta value, indicating its stability in solution, as high zeta values create strong electrostatic repulsion and prevent


DOI: 10.1021/acs.bioconjchem.5b00144
Bioconjugate Chem. 2015, 26, 1086−1094

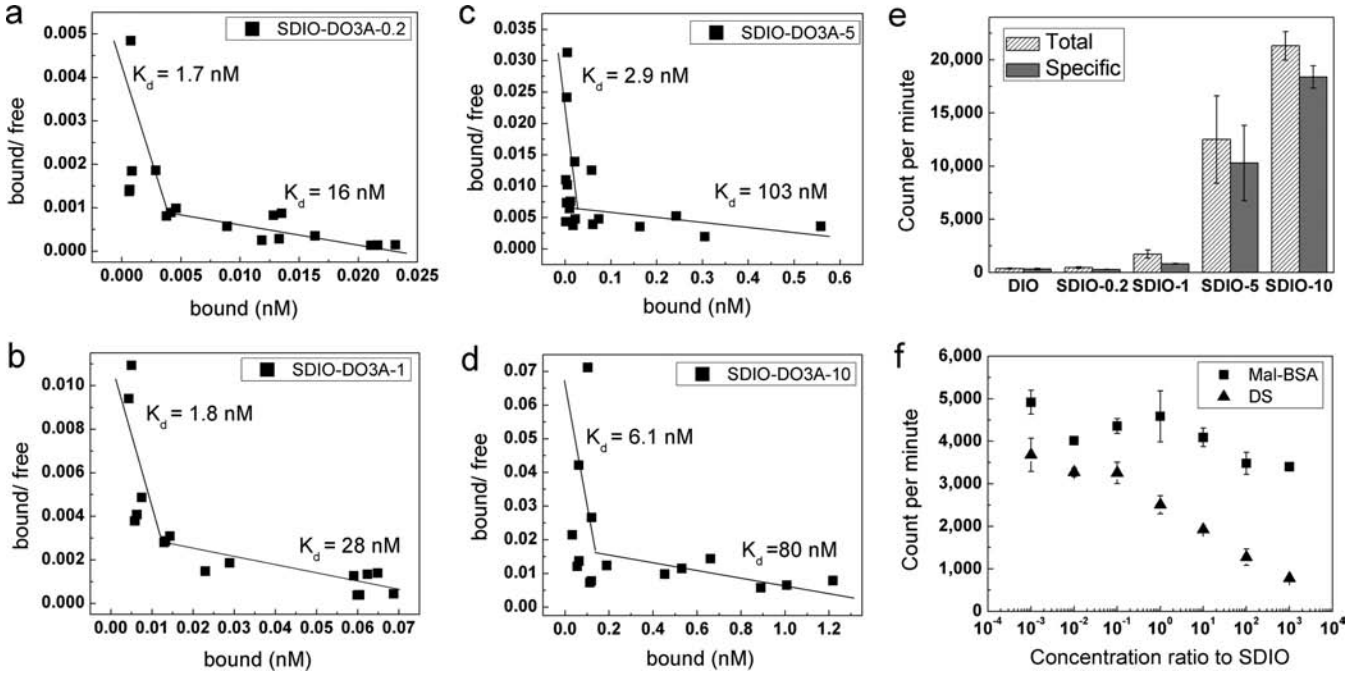


**Figure 2.** $^{111}In^{3+}$-radiolabeled nanoparticle binding studies at 4 °C. (a–d) Scatchard plots of SDIO–DO3A nanoparticles of four sulfation levels binding to SR-A on cell surfaces. The biphasic plots observed for all of the sulfated nanoparticles suggested two different binding sites on the receptors with different affinities. (DIO–DO3A can barely bind to the SR-A as displayed in panel e, so its Scatchard plot is not shown.) (e) Gamma counts of total and specific binding of SDIO–DO3A nanoparticles of different degrees of sulfation (at 1 mM [Fe]) to scavenger class A receptors. The more highly sulfated nanoparticles label cells more effectively. (f) Competitive inhibition study of binding to SR-A for SDIO–DO3A-1 using competitors mal-BSA or dextran sulfate. A single SDIO–DO3A-1 concentration (100 $\mu$M [Fe] or 22 nM [SDIO]) was used for incubation, while various concentrations of competitor covered 7 orders of magnitude in molar ratio. Error bars represent SEM ($n$ = 3). Full inhibition can be achieved with dextran sulfate, and only partial inhibition, by mal-BSA, suggesting that the binding site for dextran sulfate and the nanoparticles might partially overlap with that for mal-BSA.

aggregation resulting from collisions caused by Brownian motion.[28]

The relaxivity values, $r_1$ and $r_2$, were in a similar range for different SDIO–DO3A nanoparticles ($r_1$ = 14–16 $mM^{-1}$ $s^{-1}$, and $r_2$ = 70–90 $mM^{-1}$ $s^{-1}$) and DIO–DO3A ($r_1$ = 17.9 $mM^{-1}$ $s^{-1}$, and $r_2$ = 103.3 $mM^{-1}$ $s^{-1}$; Figure S2, all values per iron concentration), with core sizes of 6 nm, but both $r_1$ and $r_2$ relaxivity decreased with a higher sulfation level. This could be the result of increased thickness of the coating for the more negative surfaces; the coating may physically exclude protons from the coating and reduce residence time within the coating zone, thus modulating relaxivity.[29] The high $r_2/r_1$ ratio, which is larger than 5, suggests that SDIO–DO3A could be used preferably as a $T_2$*-weighted MRI contrast agent. Relaxivity per particle was ~$3.6 \times 10^5$ $mM^{-1}$ $s^{-1}$ for SDIO–DO3A and $4.5 \times 10^5$ $mM^{-1}$ $s^{-1}$ for DIO–DO3A (one particle contains ~4500 iron ions), supporting the notion that the nanoparticles will be effective contrast agents.

**MRI Studies.** $T_2$-weighted images of various concentrations of the SDIO–DO3A nanoparticles in PBS solutions were obtained from a 7 T magnet at room temperature (Figure 1c). At the same iron concentrations, these nanoparticles showed a similar ability to generate contrast in MR images, as expected. This indicates that imaging contrast is more related to the concentration of iron oxide, with little influence from the surface coating or hydrodynamic size. The $r_2$ of five samples at 7 T and room temperature were (Figure S3, all values as per iron concentration) 198 $mM^{-1}$ $s^{-1}$ (DIO–DO3A), 189 $mM^{-1}$ $s^{-1}$ (SDIO–DO3A-0.2), 161 $mM^{-1}$ $s^{-1}$ (SDIO–DO3A-1), 154 $mM^{-1}$ $s^{-1}$ (SDIO–DO3A-5), and 143 $mM^{-1}$ $s^{-1}$ (SDIO–DO3A-10). The values at 7 T were almost doubled compared to that at 1.4 T, and the trend that more highly sulfated nanoparticles had a smaller $r_2$ was also observed in 7 T systems.

**Binding Studies.** Binding assays have been developed mainly for proteins or peptides. We adapted a method using Scatchard analysis to assay binding affinity of the targeted nanomaterials for SR-A receptors. We chose $^{111}In^{3+}$ to radiolabel the probes to take advantage of its relatively long half-life (2.8 days), high gamma emission efficiency, and easy chelation by DO3A (log $K$ > 25).[30] Using Scatchard plots of bound/free vs bound for SDIO–DO3A nanoparticles (Figure 2a–d), we calculated the dissociation constants for the different degrees of sulfation. Linear plots were observed for all of the studies, indicating that there were no cooperativity effects. The plots showed biphasic character, suggesting that the nanoparticles interacted with more than one binding site, with differing affinities, on the receptor. In general, increasing the sulfation of the nanoparticles had little effect on the $K_d$ for the site of higher binding affinity; for the site with lower binding affinity, there was a decrease in affinity for the more highly sulfated particles: SDIO–DO3A-0.2 and SDIO–DO3A nanoparticles had perhaps slightly lower dissociation constants than those of more highly sulfated analogues. This implies that sulfation level is not the only factor that influences the ability of SDIO–DO3A nanoparticles to bind to receptors. Other parameters, such as particle size and coating structure, might also change the nanoparticle's ability to interact with surface receptors. In general, all SDIO–DO3A nanoparticles had similar high binding affinity to SR-A in the nanomolar range.


DOI: 10.1021/acs.bioconjchem.5b00144
Bioconjugate Chem. 2015, 26, 1086–1094

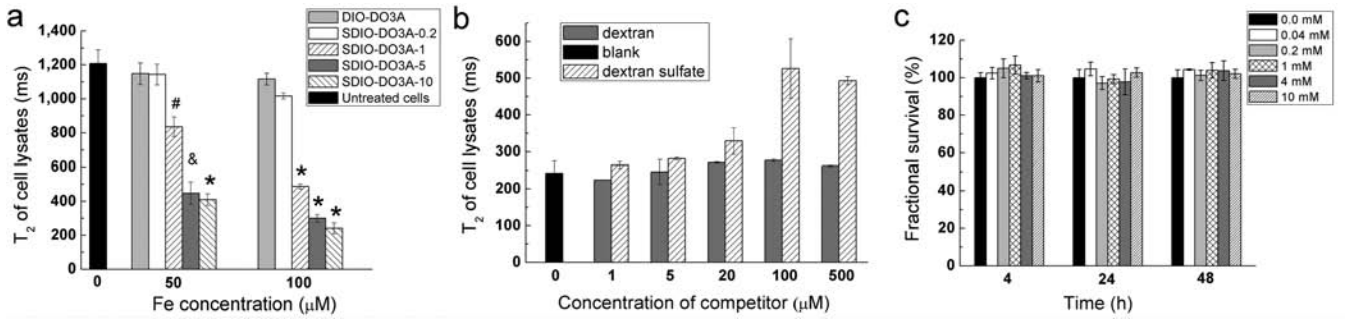


**Figure 3.** Uptake studies of SDIO−DO3A by J774 macrophages and cytotoxicity study on HepG2 cells at 37 °C. (a) Uptake studies of SDIO−DO3A at different iron concentrations at 37 °C. Mean $T_2$ values of J774 cell lysates incubated with SDIO−DO3A nanoparticles for 1 h are presented. ★, $P < 0.001$; &, $P = 0.002$; #, $P = 0.01$−$0.02$. (b) Competition uptake of SDIO−DO3A-10 (100 μM [Fe]) by J774 with the presence of competitor (dextran or dextran sulfate) at 37 °C. (c) Cell viability studies with $C_{12}$-resazurin assay. HepG2 cells were incubated for 4, 24, and 48 h with different iron concentrations of SDIO−DO3A-10. Fluorescent intensities reflecting survival fractions were normalized against the signal from the untreated cells. All error bars present SEM ($n = 3$).

However, while the nanoparticles showed similar affinity to SR-A, the more highly sulfated nanoparticles appear to interact more avidly with cells, as evidenced by the greater accumulation of sulfated SDIO−DO3A-5 and SDIO−DO3A-10 compared to that of their less and nonsulfated counterparts (Figure 2e). There is a clear trend that higher sulfation levels improve the deposition of nanoparticles on the cells (using chilled cells to restrict endocytosis). While affinity and avidity often scale together when describing antibodies, the system for which these terms were developed, the nanoparticle system, may differ. As relatively large charged bodies, the more highly negatively charged nanoparticles perhaps experience fewer nonspecific interactions with the negatively charged cell surface, allowing for more frequent opportunities to bind SR-A.

Particularly notable is the much greater binding of the more highly sulfated SDIO−DO3A-5 and SDIO−DO3A-10 to cells compared to that of DIO−DO3A (Figure 2e). DIO has been reported in the literature to label inflamed plaques by nonspecific phagocytosis by macrophages. Our results demonstrate that sulfated dextran coatings increase macrophage labeling by iron oxide nanoparticles by about 60-fold; this could have a major impact on clinical application and suggests that lower doses of SDIO−DO3A could be used to label plaques *in vivo* with potentially less off-target activity.

We used competition studies to further investigate the multiple binding sites suggested by the Scatchard plots. SR-A can recognize a broad range of polyanionic ligands that can share the same binding sites and overlapping binding sites for some ligands, as verified by nonreciprocal cross-competition of ligands.[31] For example, although oxidized low density lipoprotein (ox-LDL) inhibits the binding of acetylated LDL (ac-LDL) by SR-A completely, ac-LDL can block that of ox-LDL only partially, suggesting the existence of two discrete but overlapping ligand binding sites on the receptor.[31−33] To examine whether two binding sites for SDIO might be at play in our system, we performed a competition study between SDIO−DO3A-1 and mal-BSA, a ligand that we have previously used to facilitate targeting to SR-A (synthesis and characterization are described in Supporting Information, Figure S4).[16] The results demonstrated that mal-BSA can only partially inhibit the binding of the SDIO−DO3A-1 (Figure 2f). However, dextran sulfate can block the binding of SDIO−DO3A-1 to cells nearly completely. This suggests that SDIO−DO3A binds to a unique site on SR-A and also shares another overlapping site with mal-BSA. The overlapping site with mal-BSA may be the lower-affinity site revealed in the Scatchard plots. Future studies will examine this in more detail.

**Cellular Uptake Studies.** Uptake of SDIO−DO3A by J774 macrophages at 37 °C was studied to evaluate the effect of charge on cellular uptake of the nanoparticles. As shown in Figure 3a, a clear trend of decreasing $T_2$ values for cells incubated with increasing concentrations of SDIO−DO3A nanoparticles is observable. There is significantly less uptake of the untargeted DIO−DO3A (gray bar) at both 50 and 100 μM. Furthermore, the degree of sulfation clearly affected uptake; with increasing sulfation on the nanoparticles, the $T_2$ decreased dramatically for cells incubated with SDIO−DO3A. This suggests that sulfation of DIO−DO3A facilitates SR-A targeting and greatly improves uptake efficiency and accumulation of the nanoparticles in macrophages. These results are consistent with those observed in the binding studies, which showed greater levels of binding for the more highly sulfated nanoparticles. Considering that SDIO−DO3A nanoparticles with higher sulfation levels have smaller transverse relaxivities compared with those of DIO−DO3A, the increase in particle uptake efficiency for sulfated nanoparticles compared to that for nonsulfated is even greater (additional 1.4-fold). Statistical calculations confirmed significant differences between the untreated cells and those incubated with SDIO−DO3A with higher sulfation levels. The cell lysates were further imaged on the same 7 T Bruker system and demonstrated strong contrast enhancement after uptake of SDIO−DO3A with high sulfation levels (Figure S5a). A similar uptake study on the P388D1 macrophage cell line also displayed the same trend, as shown in Figure S5b.

A competition uptake study was performed with SDIO−DO3A-10 to confirm that internalization of the nanoparticles is a receptor-mediated process. With a receptor-mediated uptake process, the excess ligand, dextran sulfate, competes for binding to the SR-A on macrophages, thus greatly reducing the uptake of the SDIO−DO3A nanoparticles and resulting in a higher relaxation time of cell lysates. On the contrary, dextran, which is not a ligand for SR-A, cannot inhibit the uptake of SDIO−DO3A significantly. As shown in Figure 3b, for cells incubated with 100 μM [Fe] of SDIO−DO3A-10, competing dextran sulfate reduced the internalization of the nanoparticles and the $T_2$ increased from 242 to 526 ms (70% inhibition). Because we have previously demonstrated that the dextran sulfate itself is nontoxic to macrophages[7] and the presence of dextran sulfate with SDIO−DO3A particles does not cause toxicity (Figure


DOI: 10.1021/acs.bioconjchem.5b00144
*Bioconjugate Chem.* 2015, 26, 1086−1094

S6a, b), this supports the conclusion that the reduction of SDIO−DO3A uptake was not caused by toxicity or other influence on the cells themselves.

**Biocompatibility.** The toxicity of SDIO−DO3A-10 nanoparticles was evaluated on HepG2 liver cells and P388D1 macrophages using the $C_{12}$-resazurin viability assay. Liver cells were chosen because the iron oxide nanoparticles are normally cleared by the liver and spleen, where they are metabolized and broken down to free iron ions. Therefore, these cells may be the most vulnerable to the toxicity of breakdown products. Viability of cells after incubation with different concentrations at different incubation times was compared. Untreated cells (blank) served as the control. The results of biocompatibility on HepG2 cells are shown in Figure 3c. Fluorescent intensities reflecting survival fractions were normalized against the signal from the untreated cells. An unpaired two-tailed *t*-test was performed to compare treated cells against the control within each incubation time. With all $P > 0.2$, there is no significant difference between the untreated cells and those incubated with SDIO−DO3A-10 at concentrations up to 10 mM. The same assay was performed on macrophages, which are the ideal targets of the nanoparticles, exhibiting similar results (Figure S7). These results indicate that SDIO−DO3A does not have observable toxicity to mammalian cells, in agreement with our past experience.

## DISCUSSION

Scavenger receptor class A has been known for its role in immune responses. SR-A contains a characteristic collagen domain, which is responsible for ligand binding, and this domain is found only in SR-A, compared with other scavenger receptors.[33−37] SR-A recognizes a broad range of polyanionic macromolecules but not all polyanionic molecules; thus, there appears to be a structural as well as charge dependence for receptor binding.[9,10,33,38] Recognized ligands include modified low density lipoprotein (ox-LDL, acetyl-LDL), polyribonucleotides (poly-G and poly-I), polysaccharides (dextran sulfate, fucoidan), and others.[33,35−38]

The SDIO−DO3A nanoparticles are designed based on the fact that dextran sulfate is a known ligand for SR-A, more specifically, SR-AI/II.[37,38] Through literature examination, we found that the only other receptors reported to bind dextran sulfate are SR-C, found only on insect cells,[34,37] and LOX-1. LOX-1 is listed by Canton et al. in their review to recognize dextran sulfate.[34] LOX-1 may be found on platelets and macrophages after stimulation by lipopolysacchrides or tumor necrosis factor, but the expression of LOX-1 by macrophages without induction is negligible compared to the high expression of SR-A, which is on the order of $5 \times 10^5$ per cell.[16,37] Tani et al. showed that LOX-1 was not expressed on P388D1 cells, and Moriwaki et al. demonstrated that LOX-1 is barely expressed by murine peritoneal macrophages without stimulation.[39,40] In the unstimulated P388D1 and J774 cell systems used in this work, SR-A is the primary receptor available to bind SDIO. However, as noted, there may be a neglible amount of LOX-1 present, which may contribute to the biphasic character of the Scatchard plot. To isolate contribution from SR-A only, in the future, we will perform studies in transfected cells lines that express SR-A and compare these to untransfected cells of the same background without SR-A.

In this work, we hypothesized that increased sulfation/anionic character might improve binding and/or uptake of SDIO−DO3A. It was demonstrated successfully that increasing surface sulfation, thus resulting in a more negative zeta potential for the nanoparticles, increased uptake and binding. We had previously observed similar trends for another ligand to SR-A, maleylated-BSA, in which increasing the amount of negative maleyl groups improved uptake of mal-BSA by macrophages. Optimal uptake was observed for 80% maleylation and above.[16] SR-A is a somewhat promiscuous receptor in that it recognizes polynionic ligands but not all polyanionic molecules; for example, poly-I and poly-G are recognized but not poly-A, -T, or -C.[33,35,36,38] It appears that anionic character is not the only factor that affects binding and uptake, and there must be some structural component for how that charge is presented as well. In the current studies of dextran sulfate and our previous studies on mal-BSA, we have observed that increasing negative charge for these ligands improves uptake and binding.

SDIO−DO3A nanoparticles are designed to target activated macrophages accumulated in the inflamed atherosclerotic plaques for *in vivo* multimodal imaging. Although Kupffer cells and some other tissue macrophages may also express SR-A, the specificity for atherogenic macrophages lies in geographic segregration because normal vessel walls do not contain macrophages. In our previous studies on *in vivo* imaging of inflamed atherosclerotic plaques in mouse and rat carotid injury models, no PET signal or enhanced MRI contrast was observed on vessel walls of the uninjured contralateral carotid artery.[6] However, PET signal correlated to the injured carotid artery, with elevated MRI contrast showing a detailed pattern of macrophage distribution on the vessel wall. This suggested that activated macrophages expressing SR-A can be targeted by these probes with negligible off-target labeling of normal lumen.

## CONCLUSIONS

In summary, we have developed iron oxide-based nanoparticles for macrophage imaging and demonstrated that nanoparticles displaying ligands to SR-A bind to these receptors with similar affinity as that of the free ligands and that greater negative surface charge improves uptake by macrophages without causing toxicity to liver cells. Thus, attachment of SR-A ligands to nanoparticles does not appear to adversely affect ligand function. Furthermore, the probes generate good contrast in MR images. Scatchard analysis, a commonly employed tool in the biochemical/biological sciences, was adapted to allow quantitative comparison of nanoparticle binding to their target. To date, reports of targeted nanoparticles for imaging have largely demonstrated efficacy primarily through qualitative measures such as changes in image intensity.[3,41] A few reports have attempted more rigorous quantitative approaches using competitive $IC_{50}$ determination,[42,43] but $IC_{50}$ determinations rely on a number of assumptions, including a lack of cooperative binding. Scatchard analysis, on the other hand, can reveal cooperative binding, which produces nonlinear plots,[44−46] and thus may be a more robust choice for assessment of nanomaterial binding properties. Our detailed binding studies provide insight into how targeted materials can bind to biomarkers and offer a possible standard to compare different imaging probes used for similar purposes. In future studies, we will further refine this method for more precise calculation of nanoparticle mass and higher accuracy in binding affinity.

Although increasing numbers of nanoparticle-based imaging probes are being reported in the literature, few articles comprehensively investigate their biological behavior and


DOI: 10.1021/acs.bioconjchem.5b00144
*Bioconjugate Chem.* 2015, 26, 1086−1094

their advantages over existing materials.[47] Intensive biological assays or cytometric analysis are highly desirable for elucidating macrophage biology. In the future, similar research related to the biological properties of probes could be performed to optimize probe efficiency so that a minimal dose could be administrated to avoid side effects and toxicity, which is critical for clinical translation.

## EXPERIMENTAL SECTION

**Synthetic Materials and Methods.** General materials and synthetic details are described in the Supporting Information.

**Characterizations of SDIO−DO3As.** Successful sulfation was verified by infrared spectroscopy with a Shimadzu IR Prestige 21 spectrophotometer. The samples were also sent to Columbia Analytical Service, Tucson, Arizona, for sulfur content analysis by combustion-infrared spectroscopy. The amount of iron in SDIO−DO3A was measured with a Varian AA 220FS atomic absorption spectrophotometer using an air/acetylene flame. The core sizes of DIO−DO3A and SDIO−DO3A were measured by transmission electron microscopy (TEM), using a Philips CM-12 operating at 80 kV. Sample solutions (5 $\mu$L) were loaded on a thin carbon film, 400 copper mesh grids, and dried naturally. The average core diameter of particles was calculated based on 500 particles from different regions on the grids. The average hydrodynamic diameters and size distributions were measured by dynamic light scattering (DLS) using a Nanotrac 150 particle size analyzer (Microtrac, Montgomeryville, PA, USA). The zeta potential of SDIO−DO3A was obtained by determining the electrophoretic mobility of the particles using a Malvern Zetasizer in both deionized water and PBS (1×) at room temperature.

Longitudinal ($T_1$) and transverse ($T_2$) relaxation times of SDIO−DO3A in PBS solution with different iron concentrations were measured at 60 MHz (1.4 T) and 37 °C on a Bruker Minispec mq60 (Bruker, Billerica, MA, USA), as reported previously.[7] The stock solutions of SDIO−DO3A were prepared at 0.1, 0.2, 0.3, 0.4, and 0.5 mM [Fe]. Each solution was incubated at 37 °C for 8−10 min before measurement to reach the thermal equilibrium. $T_1$ values were determined with an inversion recovery sequence with 10−15 data points, whereas $T_2$ values were measured using a Carr−Purcell−Meiboom−Gill sequence, with $\tau$ = 1 ms and 200 data points. The longitudinal ($r_1$) and transverse ($r_2$) relaxivities were determined as the slope of the linear plots of $1/T_1$ or $1/T_2$ vs iron concentration, with a correlation coefficient greater than 0.99.

**MRI Studies.** MR images were obtained from Bruker Advance Biospec system (Billericia, MA, USA) equipped with a 95 mT/m max gradient set and 72 mm i.d. coil operating at 300 MHz, at ambient temperature (25 °C). $T_2$-weighted images of DIO−DO3A and SDIO−DO3A in PBS solutions with iron concentrations of 67.5, 125, 250, and 500 $\mu$M were acquired using a spin−echo sequence, with a repetition time (TR) of 5000 ms and various echo time (TE). In all experiments, the FOV was 6 × 6 cm$^2$, matrix size was 128 × 128, and slice thickness was 1 mm. The $T_2$ values of each sample were obtained by taking images of various TE, drawing the ROIs, and fitting the curve for $T_2$ relaxation. The transverse relaxivity ($r_2$) at 7 T was then determined as the slope of the linear plots of $1/T_2$ vs iron concentration, with a correlation coefficient greater than 0.98.

MRI *in vitro* studies with cell lysates of SDIO−DO3A were also performed on the Bruker Advance Biospec system. Cell lysates were prepared from the uptake study mentioned above. A $T_2$-weighted image of cell lysates was obtained using MSME sequence, with a TR of 1344 ms and various TE. In all experiments, the FOV was 6 × 6 cm$^2$, matrix size was 128 × 128, and slice thickness was 1 mm. The $T_2$ values of each sample were obtained with the same method.

**Binding Affinity.** To label the particles with $^{111}In^{3+}$, SDIO−DO3A (1.6 mg) was dissolved in 100 $\mu$L of 0.2 M, pH 5.5, sodium acetate−acetic acid buffer solution in a 1.5 mL Eppendorf vial. $^{111}InCl_3$ (∼200 $\mu$Ci) was added to the vial; then, the mixture was vortexed for 5 s to obtain a uniform solution, which was incubated at 90−100 °C for 45 min to allow the chelation of $^{111}In$ to DO3A. Ethylenediaminetetraacetic acid (EDTA) aqueous solution (10 $\mu$L, 100 mM) was then added to chelate the free $In^{3+}$ ions with a further incubation at 90−100 °C for 15 min. The crude product was purified by centrifuge filtration with 10K Da Nanosep filtration tube (Millipore Inc., Billerica, MA, USA) at 14 000 rpm for 15 min and washed three times with pH 5.5 buffer solutions (100 $\mu$L). The product was then recovered by centrifugation at 10 000 rpm for 2 min. SDIO−$^{111}In^{3+}$−DO3A (∼15 $\mu$L) was diluted with $CO_2$-independent media for an iron concentration of 1 mM. This stock solution was further diluted to the following concentrations for binding studies: 0.3, 1, 3, 10, 30, 100, and 300 $\mu$M [Fe].

J774 macrophages were distributed with RPMI 1640 (containing 10% lipoprotein-deficient bovine serum) into 24-well plates at a population of 1 × 10$^5$ and incubated overnight (0.4 mL per well). RPMI 1640 was then removed and replaced with $CO_2$-independent medium (prewarmed at 37 °C). The cells were adapted to cold, to suppress endocytosis, by placement in 4 °C on crushed ice for 15 min. The medium was then replaced with the radiolabeled probe ($^{111}$In-radiolabeling procedure described in Supporting Information) at different concentrations in cold $CO_2$-independent media for a 1 h incubation at 4 °C in fridge. When the probe was removed, cells were washed with 0.5 mL of DPBS three times and lysed in 0.5 mL of deionized water. Lysates were transferred into gamma counting tubes. Specific binding was obtained by performing the assay with the presence of 3 mg/mL (45.5 $\mu$M) bovine serum albumin. The excess BSA occupies nonspecific binding sites and leaves the specific binding sites for the radiolabeled probe. The dissociation constant $K_d$ for SDIO−DO3A then was calculated using Scatchard analysis of plots of bound/free vs bound. To determine the number of moles of nanoparticles in a given weight/volume, we calculated the molecular weight of the SDIO−DO3A nanoparticles from the core size, density, and iron percentage of our iron oxide, as described in the Supporting Information in detail.

Competition binding studies using the competitive binders, dextran sulfate or maleylated BSA (mal-BSA), were performed on J774 macrophages. Maleylated BSA was synthesized as previously reported and briefly described in Supporting Information.[16] The cells were cultured, distributed into 24-well plates, and conditioned to cold at 4 °C on crushed ice as above. A single SDIO−DO3A-1 concentration (100 $\mu$M [Fe] or 22 nM [SDIO]) was used for incubation in all wells, and various concentrations of competitor, mal-BSA or dextran sulfate, covered 7 orders of magnitude in molar ratio (from 0.001- to 1000-fold of [SDIO]). The cells were washed and lysed in the same way as above, and radioactivity was measured by gamma counter.


DOI: 10.1021/acs.bioconjchem.5b00144
*Bioconjugate Chem.* 2015, 26, 1086−1094

**Cellular Uptake Studies.** To study the specific cellular uptake of SDIO−DO3A nanoparticles by macrophages, J774 cells were plated into 6-well culture plates at a concentration of $5 \times 10^5$ cell/mL in RPMI 1640 with 10% lipoprotein-deficient bovine serum (2 mL per well). Cells were incubated at 37 °C (5% $CO_2$) overnight to adhere to the bottom of the dishes. Solutions of different SDIO−DO3A nanoparticles at 50 and 100 $\mu$M [Fe] were prepared by dissolving nanoparticles in RPMI 1640 with 1% L-glutamine and 10% LPDS. The medium was then replaced with fresh medium containing SDIO−DO3A sand incubated for 1 h. After removal of the SDIO−DO3A solutions, cells were washed with 2 mL of DPBS three times. Deionized water (~1 mL) was then added, and the freeze/thaw (30 min/20 min) method was repeated twice to lyse cells. Cell lysates were lyophilized, and DI water (0.3 mL) was added to the residue to prepare the solution for $T_2$ measurement by the Bruker Minispec mq60. A similar study was also performed on P388D1 cells to confirm the nanoparticles' targeting to SR-A using different macrophage lines. Competition uptake experiments were performed to prove that cellular uptake was receptor-mediated. The J774 cells were incubated with SDIO−DO3A-10 ([Fe] = 50 $\mu$M) in the presence of competing dextran sulfate or noncompeting dextran as the control at 0, 1, 5, 20, 100, and 500 $\mu$M. After 1 h incubation at 37 °C in a 5% $CO_2$ atmosphere, cells were washed three times with DPBS and lysed with DI water. The lysates were then prepared for relaxation time measurements as above.

**Biocompatibility.** Biocompatibility of SDIO−DO3A-10 was evaluated on HepG2 and P388D1 macrophages using $C_{12}$-resazurin viability assays. HepG2 cells were maintained in minimum essential medium supplemented with 10% FBS, 200 U/mL penicillin, 200 $\mu$g/mL streptomycin, 1 mM sodium pyruvate, and 1 mM nonessential amino acids at 37 °C in a humidified 5% $CO_2$ atmosphere. P388D1 cells were maintained in RPMI 1640 with L-glutamine and 10% FBS. To perform the viability experiments, HepG2 or J774 cells were plated in 96-well plates at a concentration of $10^4$ cells per well and incubated in a 5% $CO_2$ atmosphere at 37 °C overnight. The medium was then replaced with fresh media containing varying concentrations of SDIO−DO3A-10 (at 0.04, 0.2, 1, 4, 10 mM [Fe]) and incubated for 4, 24, or 48 h. The medium was then removed, and cells were washed with DPBS three times. Media containing $C_{12}$-resazurin (5 $\mu$M) was then added to the wells, and after a 15 min incubation, fluorescence was measured by a Safire$^2$ monochromator microplate reader (Tecan Austria, Groedig, Austria) with excitation at 563 nm and emission at 587 nm.

## ■ ASSOCIATED CONTENT

### Supporting Information

Synthetic details, characterization (calculations for the molecular weight of nanoparticles, linear fitting for relaxivities), and *in vitro* study information (biocompatibility study and uptake study). The Supporting Information is available free of charge on the ACS Publications website at DOI: 10.1021/acs.bioconjchem.5b00144.

## ■ AUTHOR INFORMATION

### Corresponding Author

*E-mail: aylouie@ucdavis.edu.

### Notes

The authors declare no competing financial interest.

## ■ ACKNOWLEDGMENTS

The authors wish to acknowledge the National Institutes of Health (EB008576-01 and EB000993), the Center for Molecular and Genomic Imaging at the University of California, Davis (U24 CA 110804), and the NMR award of the University of California, Davis for support of this work. We thank J. Walton and F. Hayes for their help with MRI and TEM, respectively.

## ■ ABBREVIATIONS

SR-A, scavenger receptor class A; DIO, dextran-coated iron oxide; SDIO, sulfated dextran-coated iron oxide; DO3A, 1,4,7,10-tetraazacyclododecane-1,4,7-triacetic acid; SDIO−DO3A-$x$ ($x$ = 0.2, 1, 5, 10), sulfated dextran-coated iron oxide−DO3A derivative, with numbers indicating the reaction ratio of sulfur trioxide to hydroxyls on dextran

## ■ REFERENCES

(1) Lee, D.-E., Koo, H., Sun, I.-C., Ryu, J. H., Kim, K., and Kwon, I. C. (2012) Multifunctional nanoparticles for multimodal imaging and theragnosis. *Chem. Soc. Rev. 41*, 2656−72.

(2) Thomas, R., Park, I.-K., and Jeong, Y. Y. (2013) Magnetic iron oxide nanoparticles for multimodal imaging and therapy of cancer. *Int. J. Mol. Sci. 14*, 15910−30.

(3) Choi, H. S., Liu, W., Liu, F., Nasr, K., Misra, P., Bawendi, M. G., et al. (2009) Design considerations for tumour-targeted nanoparticles. *Nat. Nanotechnol. 5*, 42−7.

(4) Tassa, C., Shaw, S. Y., and Weissleder, R. (2011) Dextran-coated iron oxide nanoparticles: a versatile platform for targeted molecular imaging, molecular diagnostics, and therapy. *Acc. Chem. Res. 44*, 842−52.

(5) Amstad, E., Zurcher, S., Mashaghi, A., Wong, J. Y., Textor, M., and Reimhult, E. (2009) Surface functionalization of single superparamagnetic iron oxide nanoparticles for targeted magnetic resonance imaging. *Small 5*, 1334−42.

(6) Jarrett, B. R., Correa, C., Ma, K. L., and Louie, A. Y. (2010) In vivo mapping of vascular inflammation using multimodal imaging. *PLoS One 5*, e13254.

(7) Tu, C., Ng, T. S., Sohi, H. K., Palko, H. A., House, A., Jacobs, R. E., et al. (2011) Receptor-targeted iron oxide nanoparticles for molecular MR imaging of inflamed atherosclerotic plaques. *Biomaterials 32*, 7209−16.

(8) Jarrett, B. R., Frendo, M., Vogan, J., and Louie, A. Y. (2007) Size-controlled synthesis of dextran sulfate coated iron oxide nanoparticles for magnetic resonance imaging. *Nanotechnology 18*, 035603.

(9) de Winther, M. P. J., van Dijk, K. W., Havekes, L. M., and Hofker, M. H. (2000) Macrophage scavenger receptor class A: a multifunctional receptor in atherosclerosis. *Arterioscler., Thromb., Vasc. Biol. 20*, 290−7.

(10) Hughes, D. A., Fraser, I. P., and Gordon, S. (1995) Murine macrophage scavenger receptor: in vivo expression and function as receptor for macrophage adhesion in lymphoid and non-lymphoid organs. *Eur. J. Immunol. 25*, 466−73.

(11) Raynal, I., Prigent, P., Peyramaure, S., Najid, A., Rebuzzi, C., and Corot, C. (2004) Macrophage endocytosis of superparamagnetic iron oxide nanoparticles: mechanisms and comparison of ferumoxides and ferumoxtran-10. *Invest. Radiol. 39*, 56−63.

(12) Chao, Y., Makale, M., Karmali, P. P., Sharikov, Y., Tsigelny, I., Merkulov, S., et al. (2012) Recognition of dextran-superparamagnetic iron oxide nanoparticle conjugates (feridex) via macrophage scavenger receptor charged domains. *Bioconjugate Chem. 23*, 1003−9.

(13) Goldstein, J. L., Brown, M. S., Anderson, R. G., Russell, D. W., and Schneider, W. J. (1985) Receptor-mediated endocytosis: concepts emerging from the LDL receptor system. *Annu. Rev. Cell Biol. 1*, 1−39.

(14) Harwood, J. H., and Pellarin, L. (1997) Kinetics of low-density lipoprotein receptor activity in Hep-G2 cells: derivation and validation of a Briggs−Haldane-based kinetic model for evaluating receptor-



DOI: 10.1021/acs.bioconjchem.5b00144
*Bioconjugate Chem.* 2015, 26, 1086−1094

mediated endocytotic processes in which receptors recycle. *Biochem. J. 323*, 649−59.
(15) Murphy, J. E., Tedbury, P. R., Homer-Vanniasinkam, S., Walker, J. H., and Ponnambalam, S. (2005) Biochemistry and cell biology of mammalian scavenger receptors. *Atherosclerosis 182*, 1−15.
(16) Gustafsson, B., Youens, S., and Louie, A. Y. (2006) Development of contrast agents targeted to macrophage scavenger receptors for MRI of vascular inflammation. *Bioconjugate Chem. 17*, 538−47.
(17) Shokeen, M., and Anderson, C. J. (2009) Molecular imaging of cancer with copper-64 radiopharmaceuticals and positron emission tomography (PET). *Acc. Chem. Res. 42*, 832−41.
(18) Ping, L. W., Meyer, L. A., Capretto, D. A., Sherman, C. D., and Anderson, C. J. (2008) Receptor-binding, biodistribution, and metabolism studies of $^{64}$Cu−DOTA−cetuximab, a PET-imaging agent for epidermal growth-factor receptor-positive tumors. *Cancer Biother. Radiopharm. 23*, 158−71.
(19) Clarke, E. T., and Martell, A. E. (1991) Stabilities of trivalent metal ion complexes of the tetraacetate derivatives of 12-, 13- and 14-membered tetraazamacrocycles. *Inorg. Chim. Acta 190*, 37−46.
(20) Jarrett, B. R., Gustafsson, B., Kukis, D. L., and Louie, A. Y. (2008) Synthesis of Cu-64-labeled magnetic nanoparticles for multimodal imaging. *Bioconjugate Chem. 19*, 1496−504.
(21) Tu, C., Ma, X., House, A., Kauzlarich, S. M., and Louie, A. Y. (2011) PET imaging and biodistribution of silicon quantum dots in mice. *ACS Med. Chem. Lett. 2*, 285−8.
(22) Takács, A., Napolitano, R., Purgel, M. l., Bényei, A. C., Zékány, L. s., Brücher, E., et al. (2014) Solution structures, stabilities, kinetics, and dynamics of DO3A and DO3A−sulphonamide complexes. *Inorg. Chem. 53*, 2858−72.
(23) Cai, H. Z., and Kaden, T. A. (1994) Metal complexes with macrocyclic ligands. Part XXXVI. Thermodynamic and kinetic studies of bivalent and trivalent metal ions with 1,4,7,10-tetraazacyclododecane-1,4,7-triacetic acid. *Helv. Chim. Acta 77*, 383−98.
(24) Wangler, C., Wangler, B., Eisenhut, M., Haberkorn, U., and Mier, W. (2008) Improved syntheses and applicability of different DOTA building blocks for multiply derivatized scaffolds. *Bioorg. Med. Chem. 16*, 2606−16.
(25) Lee, H., Yu, M. K., Park, S., Moon, S., Min, J. J., Jeong, Y. Y., et al. (2007) Thermally cross-linked superparamagnetic iron oxide nanoparticles: synthesis and application as a dual imaging probe for cancer in vivo. *J. Am. Chem. Soc. 129*, 12739−45.
(26) Arungundram, S., Al-Mafraji, K., Asong, J., Leach, F. E., III, Amster, I. J., Venot, A., et al. (2009) Modular synthesis of heparan sulfate oligosaccharides for structure− activity relationship studies. *J. Am. Chem. Soc. 131*, 17394−405.
(27) Tu, C., Ng, T. S., Jacobs, R. E., and Louie, A. Y. (2014) Multimodality PET/MRI agents targeted to activated macrophages. *J. Biol. Inorg. Chem. 19*, 247−58.
(28) Obeidat, W. M., Schwabe, K., Muller, R. H., and Keck, C. M. (2010) Preservation of nanostructured lipid carriers (NLC). *Eur. J. Pharm. Biopharm. 76*, 56−67.
(29) Xie, J., Liu, G., Eden, H. S., Ai, H., and Chen, X. (2011) Surface-engineered magnetic nanoparticle platforms for cancer imaging and therapy. *Acc. Chem. Res. 44*, 883−92.
(30) Riesen, A., Kaden, T. A., Ritter, W., and Mäcke, H. R. (1989) Synthesis and X-ray structural characterisation of seven co-ordinate macrocyclic $In^{3+}$ complexes with relevance to radiopharmaceutical applications. *J. Chem. Soc., Chem. Commun.*, 460−2.
(31) Krieger, M. (1994) Structures and functions of multiligand lipoprotein receptors: macrophage scavenger receptors and LDL receptor-related protein (LRP). *Annu. Rev. Biochem. 63*, 601−37.
(32) Ashkenas, J., Penman, M., Vasile, E., Acton, S., Freeman, M., and Krieger, M. (1993) Structures and high and low affinity ligand binding properties of murine type I and type II macrophage scavenger receptors. *J. Lipid Res. 34*, 983−1000.
(33) Platt, N., and Gordon, S. (2001) Is the class A macrophage scavenger receptor (SR-A) multifunctional?—The mouse's tale. *J. Clin. Invest. 108*, 649−54.
(34) Canton, J., Neculai, D., and Grinstein, S. (2013) Scavenger receptors in homeostasis and immunity. *Nat. Rev. Immunol. 13*, 621−34.
(35) Doi, T., Higashino, K.-I., Kurihara, Y., Wada, Y., Miyazaki, T., Nakamura, H., et al. (1993) Charged collagen structure mediates the recognition of negatively charged macromolecules by macrophage scavenger receptors. *J. Biol. Chem. 268*, 2126−33.
(36) Acton, S. L., Scherer, P. E., Lodish, H. F., and Krieger, M. (1994) Expression cloning of SR-BI, a CD36-related class B scavenger receptor. *J. Biol. Chem. 269*, 21003−9.
(37) Gough, P. J., and Gordon, S. (2000) The role of scavenger receptors in the innate immune system. *Microb. Infect. 2*, 305−11.
(38) Ben, J., Zhu, X., Zhang, H., and Chen, Q. (2015) Class A1 scavenger receptors in cardiovascular diseases. *Br. J. Pharmacol.*, DOI: 10.1111/bph.13105.
(39) Tani, F., Nishikawa, S., Yokoyama, I., Hashimoto, K., Nakamoto, M., Nomura, M., et al. (2010) Lymphoid neoplastic P388D1 cells express membrane protein candidates that discriminate among the C-terminal phylogenetic diversity in heat shock protein 70 sequences. *Mol. Immunol. 48*, 191−202.
(40) Moriwaki, H., Kume, N., Kataoka, H., Murase, T., Nishi, E., Sawamura, T., et al. (1998) Expression of lectin-like oxidized low density lipoprotein receptor-1 in human and murine macrophages: upregulated expression by TNF-$\alpha$. *FEBS Lett. 440*, 29−32.
(41) Haun, J. B., Devaraj, N. K., Hilderbrand, S. A., Lee, H., and Weissleder, R. (2010) Bioorthogonal chemistry amplifies nanoparticle binding and enhances the sensitivity of cell detection. *Nat. Nanotechnol. 5*, 660−5.
(42) Liu, Z., Cai, W., He, L., Nakayama, N., Chen, K., Sun, X., et al. (2006) In vivo biodistribution and highly efficient tumour targeting of carbon nanotubes in mice. *Nat. Nanotechnol. 2*, 47−52.
(43) Xie, J., Chen, K., Lee, H.-Y., Xu, C., Hsu, A. R., Peng, S., et al. (2008) Ultrasmall c (RGDyK)-coated $Fe_3O_4$ nanoparticles and their specific targeting to integrin $\alpha v\beta 3$-rich tumor cells. *J. Am. Chem. Soc. 130*, 7542−3.
(44) Alvarado, D., Klein, D. E., and Lemmon, M. A. (2010) Structural basis for negative cooperativity in growth factor binding to an EGF receptor. *Cell 142*, 568−79.
(45) Segerman, B., Larsson, N., Holmfeldt, P., and Gullberg, M. (2000) Mutational analysis of Op18/stathmin−tubulin-interacting surfaces binding cooperativity controls tubulin GTP hydrolysis in the ternary complex. *J. Biol. Chem. 275*, 35759−66.
(46) Byrd, J. C., and MacDonald, R. G. (2000) Mechanisms for high affinity mannose 6-phosphate ligand binding to the insulin-like growth factor II/mannose 6-phosphate receptor negative cooperativity and receptor oligomerization. *J. Biol. Chem. 275*, 18638−46.
(47) Weissleder, R., Nahrendorf, M., and Pittet, M. J. (2014) Imaging macrophages with nanoparticles. *Nat. Mater. 13*, 125−38.


DOI: 10.1021/acs.bioconjchem.5b00144
*Bioconjugate Chem.* 2015, 26, 1086−1094